Electrochemistry Communications 97 (2018) 37–41

Contents lists available at ScienceDirect

Electrochemistry Communications

journal homepage: www.elsevier.com/locate/elecom

Identifying the limiting electrode in lithium ion batteries for extreme fast charging☆

Chengyu Mao[a], Rose E. Ruther[a,*], Jianlin Li[a,b], Zhijia Du[a], Ilias Belharouak[a,*]

[a] Energy and Transportation Science Division, Oak Ridge National Laboratory, Oak Ridge, TN 37830, USA
[b] Bredesen Center for Interdisciplinary Research and Graduate Education, University of Tennessee, Knoxville, TN 37996, USA

ARTICLE INFO

Keywords:
Symmetric cell
Li-ion battery
Extreme fast charging (XFC)
Ni-rich cathode
NMC811
Electric vehicles

ABSTRACT

Lithium ion batteries that are capable of extreme fast charging (XFC) are highly desirable to accelerate adoption of electric vehicles (EVs). To identify the rate limiting factors for XFC, we used both half cells and symmetric cells to investigate the fast charging behavior of the cathode and anode separately. The symmetric cells enabled accurate measurements of charge transfer at each electrode without complications from counter electrodes. The battery materials and electrode design were comparable to the state-of-the-art for EV cells. Under these conditions, the graphite anode is the rate limiting electrode for fast charging in NMC811/Graphite pouch cells. The effective N/P ratio falls below 1.0 at high charging rates, which also causes Li plating. The use of symmetric cells in this study provides new insights to identify the limiting electrode in Li-ion batteries, especially those designated for extreme fast charging applications.

1. Introduction

Lithium-ion batteries play a central role in vehicle electrification, and impressive progress has been made to increase energy density, improve cycle life, and reduce cost [1,2]. Nevertheless, relatively slow recharge times remain a major market barrier for electric vehicles (EVs) [3]. Therefore, developing lithium ion batteries capable of extreme fast charging (XFC) is highly desirable for EV adoption [4].

Layered $LiNi_{0.8}Mn_{0.1}Co_{0.1}O_2$ (NMC811) is a positive electrode (cathode) material for next generation Li-ion batteries with high energy density. NMC811 has a reversible capacity of 190 mAh/g_{NMC} for cell voltages ≤ 4.2 V vs. graphite [5]. Structural changes [6] and the reactivity of Ni^{4+} [7] have resulted in faster capacity fade for NMC811 compared to NMC532 and NMC622. However, strategies like electrolyte formulation [8,9] and surface modification [10,11] are known to stabilize Ni-rich cathodes. Moreover, the higher Ni content in NMC811 improves the electronic conductivity and Li^+-ion diffusivity [12], which is desirable for XFC. The decrease in Co in NMC811 also lowers the materials cost and optimizes the cost-to-range ratio for EVs.

Graphite remains the active material of choice for the negative electrode (anode) due to its high capacity, low cost, and suitable voltage profile compared to Si [13] and Li metal [14]. However, lithium plating on the graphite surface occurs during fast charging [15], which is likely due to limited mass transport in electrolytes [16,17] and ion depletion [18,19]. As the electrode becomes thicker, which is the most straightforward way to increase the cell energy density, mass transport issues become more severe [20,21]. An important design criteria is the relative power performance of the cathode compared to the anode. Understanding which electrode limits rate capability is critical to make breakthroughs in power limitations and enable XFC without negatively impacting cycle life and safety.

Here, we investigated the behavior of NMC811 cathodes and graphite anodes individually under XFC conditions. By employing a Li metal reference electrode [22], we cycled both cathode/cathode and anode/anode symmetric cells through voltage windows comparable to the conditions in full cells. Symmetric cells reveal the impedance and intrinsic rate capability of each individual electrode, since the working and counter electrodes are identical [23,24]. Given the numerous materials available for lithium ion batteries and the many parameters like areal loading [25], porosity [20], and electrolyte selection [17] that can

* Corresponding authors.
E-mail addresses: rutherre@ornl.gov (R.E. Ruther), belharouaki@ornl.gov (I. Belharouak).

https://doi.org/10.1016/j.elecom.2018.10.007
Received 12 September 2018; Received in revised form 2 October 2018; Accepted 3 October 2018
Available online 04 October 2018
1388-2481/

impact XFC performance, our study provides a powerful tool to determine rate limiting factors and design a battery technology for XFC.

2. Experimental

Electrode fabrication and cell build were completed at the U.S. Department of Energy (DOE) Battery Manufacturing R&D facility at Oak Ridge National Laboratory. NMC811 cathodes and graphite anodes were coated with high loadings relevant to EV batteries: 2.2 mAh/cm^2 for NMC811 and 2.6 mAh/cm^2 for graphite. NMC622 (2.4 mAh/cm^2) and NMC532 (0.94 mAh/cm^2, 1.8 mAh/cm^2, 2.4 mAh/cm^2, and 3.6 mAh/cm^2) were coated for comparison. After calendering, the NMC811 cathodes and graphite anodes had thicknesses of 49 and 58 μm, respectively. The thickness of NMC622 was 55 μm, and the thickness of NMC 532 increased from 23 μm to 89 μm as loadings increased. The electrolyte was 1.2 M $LiPF_6$ in ethylene carbonate: ethylmethyl carbonate (EC:EMC = 3:7 by weight) for all cells, and no electrolyte additives were used. Detailed information on electrode fabrication and cell assembly were reported in our previous work [26]. Symmetric cells were assembled using only positive or negative electrodes recovered from full cells at 50% state-of-charge (SOC).

All pouch cells were tested at 30 °C with 5 psi stack pressure. Bio-Logic potentiostats were used to obtain electrochemical impedance spectra (EIS), which was taken from 500 kHz to 0.2 mHz with 6 mV sinus amplitude.

Rate performance of NMC811/graphite single layer pouch cells was measured after cell formation and degassing. The cell was discharged at a constant rate of C/5 to get the maximum discharge capacity while the charging rate varied from C/10 to 6C with a hold at 4.2 V cut-off voltage. A total time limit was imposed to guarantee that the duration of the charging step did not exceed the intended time for each C rate.

Half coin cells comprising NMC811 or graphite electrodes and lithium metal were built for comparison. NMC811 was lithiated at a constant rate of C/5 and delithiated at various rates, while graphite was delithiated at a constant rate of C/5 and lithiated at various rates to compare to the charging rate performance in the full cell.

3. Results and discussion

The NMC811/Graphite pouch cell demonstrated a high reversible capacity of 197 mAh/g_{NMC} at a slow charging rate of C/10 (Fig. 1A). However, the capacity decreased monotonically as the charging rate increased, and a charge capacity of only 141 mAh/g_{NMC} (72% remaining) was obtained using the 10-minute fast charge protocol. Interestingly, although the NMC811 cathode half cell exhibited a similar capacity of 203 mAh/g_{NMC} compared to the full cell at C/10 rate, a higher charge capacity of 163 mAh/g_{NMC} (80% remaining) was achieved at 6C rate (Fig. 1B). The voltage profiles of the graphite half cell for various rates of lithiation are displayed in Fig. 1C. A high reversible capacity of 347 mAh/$g_{Graphite}$ could be maintained up to C/3. However, only 80% of the original capacity (284 mAh/$g_{Graphite}$) could be obtained at 1C, and the remaining lithiation capacity faded rapidly to 40% (99 mAh/$g_{Graphite}$) at 6C rate. The rate performance of all three cells is summarized in Fig. 1D. Clearly, the graphite anode demonstrated worse performance at high C-rates and is the limiting factor for fast charging. In addition, the optical image (Fig. 2D) of the anode harvested from the NMC811/Graphite full cell after XFC revealed substantial Li plating. This indicates that some charge capacity at high rates resulted from lithium metal deposition instead of lithium intercalation.

To probe the intrinsic rate performance of each individual electrode and eliminate interference from counter electrodes, cathode/cathode and anode/anode symmetric pouch cells were built using electrodes harvested from full cells at 50% SOC. A lithium foil, acting as a reference electrode, was placed inside the symmetric cell [27]. Unlike many symmetric or three electrode cells that use coin cells or rely on bulky hardware and sealants, our pouch cell with large electrodes (≈100 mAh) had fewer variations and enabled reliable operation under practical conditions. All electrodes were tested in a well-controlled potential range that was close to the measured potentials in the NMC811/Graphite full cell. Both cathode and anode symmetric cells cycled well, and their voltage profiles at different rates are displayed in Figs. 2A & B. Note that no voltage hold was applied at the cut-off voltage in symmetric cells. Consistent with their behavior in half cells, the graphite anodes exhibited a faster capacity decline as the lithiation rate exceeded 1C despite stable cycling at lower rates. In contrast, the NMC811 cathode exhibited less capacity loss as the delithiation rate increased from C/10 to 4C. The areal capacities of NMC811 cathodes and graphite anodes at different rates are displayed in Fig. 2C. At a low rate of C/10, the cathode exhibited an areal capacity of 2.25 mAh/cm^2 while the anode areal capacity was 2.60 mAh/cm^2, yielding an N/P ratio of 1.15. However, the rapid capacity fade of graphite at high rates caused the N/P ratio to drop to 1.0 at 3C and to 0.5 at 4C. The low N/P ratio shows that there are not enough sites for Li^+ intercalation into graphite that can be accessed at high rates. This leads to the unwanted electrodeposition of lithium metal as shown in Fig. 2D. Lithium plating causes electrolyte decomposition, Li inventory loss, dendrite growth, and internal micro-shorts. To enable NMC811/Graphite full cells for XFC, the rate capability of the graphite anode must be improved to match the NMC811 cathode.

The NMC811 cathode clearly outperforms the graphite anode under non-equilibrium cycling conditions where large concentration gradients may develop at high rates. It is also informative to examine the electrode impedance under steady-state conditions. The symmetric cells provide an ideal model system to study the charge transfer behavior of each electrode individually [28]. Nyquist plots of the symmetric cell impedance at different temperatures are displayed in Figs. 3A&B. Although graphite was rate limiting during XFC, it had lower impedance at every tested temperature, indicating that charge transfer does not limit the graphite power performance. Typically, Li-ion desolvation is the rate determining step during charge transfer [23,29]. We ascribed the mid-frequency semicircle in the Nyquist plot to charge transfer and fit this semicircle to a simplified Randles cell with charge transfer resistance in parallel with double-layer capacitance. Fig. 3C shows Arrhenius relationships for both NMC811 and graphite, and the slope yields the desolvation energy at each electrode [30]. The desolvation energy on the graphite anode was 49.9 kJ/mol, consistent with reports using similar electrolytes [31]. The cathode had a slightly higher desolvation energy of 52.9 kJ/mol. The minor differences could be due to interfacial effects and/or fitting errors. Although the graphite anode has smaller charge transfer impedance, the graphite electrode thickness is greater than the NMC811 electrode thickness, which causes longer Li-ion transport distances in the electrolyte. Mass transport limitations and salt depletion are the primary reasons for poor rate capability and Li plating [19] at high charging rates.

Although the anode is the limiting electrode under XFC conditions in these NMC811/Graphite cells, the balance may shift as materials, areal capacity, and porosity change. Fig. 3D shows the charging rate capabilities of NMC532 cathodes with different areal loadings and three different NMC cathodes with similar areal loading in half cells. As the areal loading of NMC532 increases, which is desirable for high energy cells, the charge capacity at high rates decreases dramatically. On the other hand, as the cathode shifted towards more Ni-rich compositions, a better charge capacity retention was maintained under XFC conditions. More Ni-rich cathodes have greater volumetric capacity, which enables thinner electrodes to reach the same areal capacity. Thin electrodes have less severe mass transport limitations, which improves rate capability. Specifically, the NMC811 cathode with an areal loading of 2.2 mAh/cm^2 maintained 80% capacity at 6C charging rate. The NMC532 and NMC622 cathodes with areal loadings of 2.4 mAh/cm^2 only retained 49% and 56% capacity, respectively, at 6C rate.

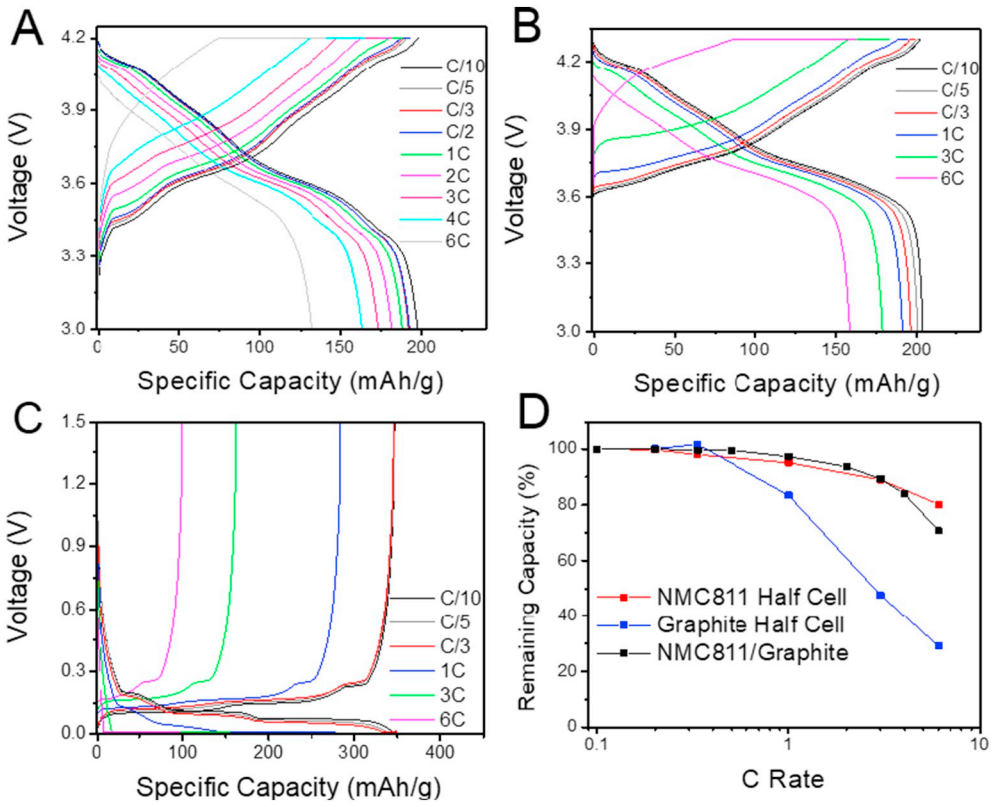

Fig. 1. (A) Voltage profiles of an NMC811/Graphite full pouch cell. The same cell was charged at various rates and discharged at C/5. (B) Voltage profiles of an NMC811 half coin cell. The NMC811 was delithiated at various rates and lithiated at C/5. (C) Voltage profiles of a graphite half coin cell. The graphite was lithiated at various rates and delithiated at C/5. (D) Rate performance of half cells and NMC811/Graphite full pouch cell.

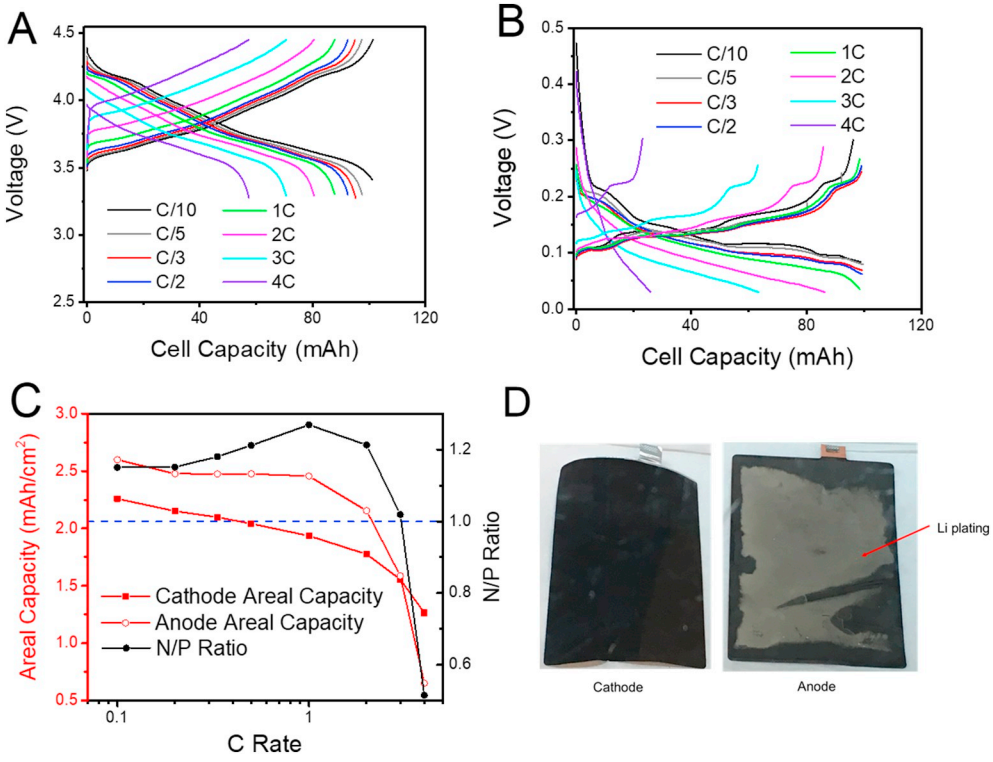

Fig. 2. (A) Voltage profiles of NMC811 in the cathode symmetric cell. The electrode was lithiated at C/5 and delithiated at various rates. (B) Voltage profiles of graphite in the anode symmetric cell. The electrode was delithiated at C/5 and lithiated at various rates. (C) Areal capacity of the NMC811 cathode and graphite anode at each rate and the resulting N/P ratio. (D) Images of electrodes from the NMC811/Graphite full cell after the charging rate performance test.

4. Conclusions

We have designed a three-electrode symmetric cell to probe the performance of the cathode and anode individually under XFC conditions. The graphite anode showed rapid capacity fade above 1C, which made it the rate limiting electrode in NMC811/Graphite full cells during XFC. Moreover, a N/P ratio ≤ 1 was reached for fast charging rates, leading to severe Li metal deposition on the anode. Since charge transfer was excluded as the cause of poor charging rate performance of the anode, other factors including mass transport in the electrolyte and salt depletion should be considered to improve the graphite performance during XFC. Given the wide range of electrode compositions

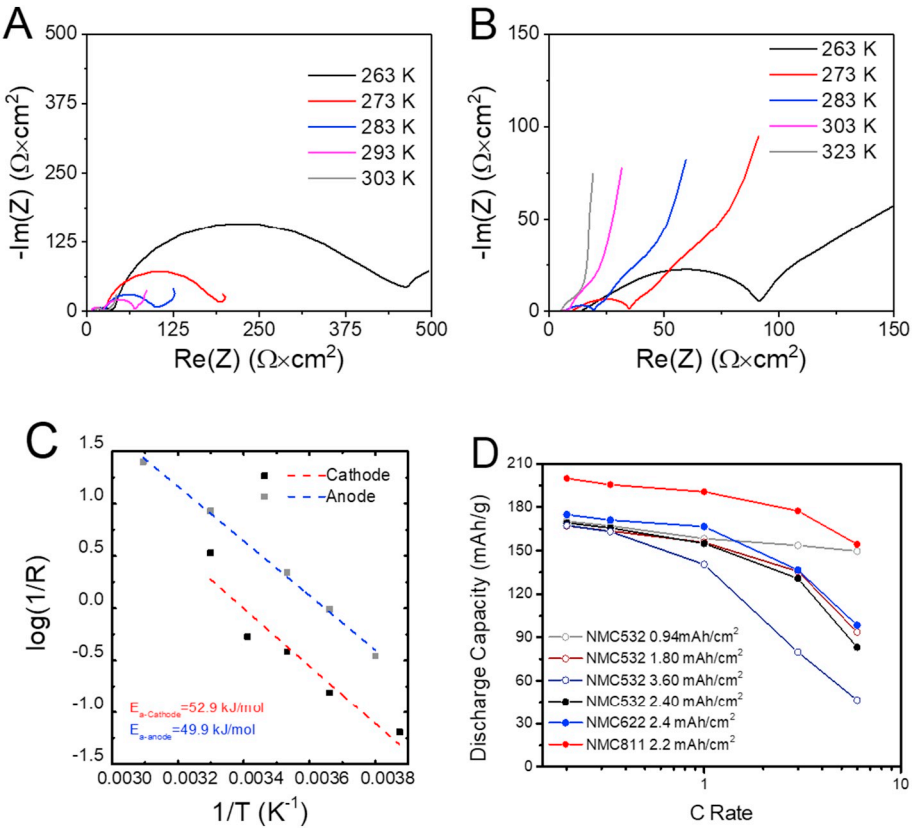

Fig. 3. EIS at different temperatures of (A) NMC811 cathode and (B) graphite anode symmetric cells. (C) Plot of resistance as a function of temperature for cathode and anode symmetric cells. (D) Rate performance of NMC532 half cells with different cathode areal loadings (empty circles) and different NMC half cells with similar areal capacities (solid circles). All NMC half cells were discharged at C/3 and charged at different rates.

combined with other factors such as electrode loading, porosity, and electrolyte formulations, our work provides new insights to identify the limiting electrode in different Li-ion batteries, especially those designated for extreme fast charging applications.

Acknowledgement

This research at Oak Ridge National Laboratory, managed by UT Battelle, LLC, for the U.S. Department of Energy (DOE) under contract DE-AC05-00OR22725, was sponsored by the Laboratory Directed Research and Development Program and by the Office of Energy Efficiency and Renewable Energy (EERE) Vehicle Technologies Office (VTO) (Deputy Director: David Howell; Applied Battery Research (ABR) Program Manager: Peter Faguy).

References

[1] S.-T. Myung, F. Maglia, K.-J. Park, C.S. Yoon, P. Lamp, S.-J. Kim, Y.-K. Sun, Nickel-rich layered cathode materials for automotive lithium-ion batteries: achievements and perspectives, ACS Energy Lett. (2016) 196–223.

[2] D.L. Wood, J. Li, C. Daniel, Prospects for reducing the processing cost of lithium ion batteries, J. Power Sources 275 (2015) 234–242.

[3] J. Li, Z. Du, R.E. Ruther, S.J. An, L.A. David, K. Hays, M. Wood, N.D. Phillip, Y. Sheng, C. Mao, S. Kalnaus, C. Daniel, D.L. Wood, Toward low-cost, high-energy density, and high-power density lithium-ion batteries, JOM 69 (2017) 1484–1496.

[4] S. Ahmed, I. Bloom, A.N. Jansen, T. Tanim, E.J. Dufek, A. Pesaran, A. Burnham, R.B. Carlson, F. Dias, K. Hardy, M. Keyser, C. Kreuzer, A. Markel, A. Meintz, C. Michelbacher, M. Mohanpurkar, P.A. Nelson, D.C. Robertson, D. Scoffield, M. Shirk, T. Stephens, R. Vijayagopal, J. Zhang, Enabling fast charging – a battery technology gap assessment, J. Power Sources 367 (2017) 250–262.

[5] C. Mao, M. Wood, L. David, S.J. An, Y. Sheng, Z. Du, H.M. Meyer, R.E. Ruther, D.L. Wood, Selecting the best graphite for long-life, high-energy li-ion batteries, J. Electrochem. Soc. 165 (2018) A1837–A1845.

[6] M.D. Radin, S. Hy, M. Sina, C. Fang, H. Liu, J. Vinckeviciute, M. Zhang, M.S. Whittingham, Y.S. Meng, A. Van der Ven, Narrowing the gap between theoretical and practical capacities in Li-ion layered oxide cathode materials, Adv. Energy Mater. 7 (2017) 1602888.

[7] R. Jung, M. Metzger, F. Maglia, C. Stinner, H.A. Gasteiger, Oxygen release and its effect on the cycling stability of $LiNi_xMn_yCo_zO_2$ (NMC) cathode materials for Li-ion batteries, J. Electrochem. Soc. 164 (2017) A1361–A1377.

[8] L.D. Ellis, J. Xia, A.J. Louli, J.R. Dahn, Effect of substituting $LiBF_4$ for $LiPF_6$ in high voltage lithium-ion cells containing electrolyte additives, J. Electrochem. Soc. 163 (2016) A1686–A1692.

[9] K. Beltrop, S. Klein, R. Nölle, A. Wilken, J.J. Lee, T.K.J. Köster, J. Reiter, L. Tao, C. Liang, M. Winter, X. Qi, T. Placke, Triphenylphosphine oxide as highly effective electrolyte additive for graphite/NMC811 lithium ion cells, Chem. Mater. 30 (2018) 2726–2741.

[10] O. Srur-Lavi, V. Mikkulainen, B. Markovsky, J. Grinblat, M. Talianker, Y. Fleger, G. Cohen-Taguri, A. Mor, Y. Tal-Yosef, D. Aurbach, Studies of the electrochemical behavior of NMC 811 electrodes coated with $LiAlO_2$, J. Electrochem. Soc. 164 (2017) A3266–A3275.

[11] K.-J. Park, B.-B. Lim, M.-H. Choi, H.-G. Jung, Y.-K. Sun, M. Haro, N. Vicente, J. Bisquert, G. Garcia-Belmonte, A high-capacity $Li[Ni_{0.8}Co_{0.06}Mn_{0.14}]O_2$ positive electrode with a dual concentration gradient for next-generation lithium-ion batteries, J. Mater. Chem. A 3 (2015) 22183–22190.

[12] H.-J. Noh, S. Youn, C.S. Yoon, Y.-K. Sun, Comparison of the structural and electrochemical properties of layered $Li[Ni_xCo_yMn_z]O_2$ (x = 1/3, 0.5, 0.6, 0.7, 0.8 and 0.85) cathode material for lithium-ion batteries, J. Power Sources 233 (2013) 121–130.

[13] M.N. Obrovac, V.L. Chevrier, Alloy negative electrodes for Li-ion batteries, Chem. Rev. 114 (2014) 11444–11502.

[14] X.B. Cheng, R. Zhang, C.Z. Zhao, Q. Zhang, Toward safe lithium metal anode in rechargeable batteries: a review, Chem. Rev. 117 (2017) 10403–10473.

[15] Q.Q. Liu, L. Ma, C.Y. Du, J.R. Dahn, Effects of the $LiPO_2F_2$ additive on unwanted lithium plating in lithium-ion cells, Electrochim. Acta 263 (2018) 237–248.

[16] K.G. Gallagher, S.E. Trask, C. Bauer, T. Woehrle, S.F. Lux, M. Tschech, P. Lamp, B.J. Polzin, S. Ha, B. Long, Q. Wu, W. Lu, D.W. Dees, A.N. Jansen, Optimizing areal capacities through understanding the limitations of lithium-ion electrodes, J. Electrochem. Soc. 163 (2015) A138–A149.

[17] D.S. Hall, A. Eldesoky, E.R. Logan, E.M. Tonita, X. Ma, J.R. Dahn, Exploring classes of co-solvents for fast-charging lithium-ion cells, J. Electrochem. Soc. 165 (2018) A2365–A2373.

[18] Z. Du, D.L. Wood, C. Daniel, S. Kalnaus, J. Li, Understanding limiting factors in thick electrode performance as applied to high energy density Li-ion batteries, J. Appl. Electrochem. 47 (2017) 405–415.

[19] H.J. Chang, A.J. Ilott, N.M. Trease, M. Mohammadi, A. Jerschow, C.P. Grey, Correlating microstructural lithium metal growth with electrolyte salt depletion in lithium batteries using (7)Li MRI, J. Am. Chem. Soc. 137 (2015) 15209–15216.

[20] B. Delattre, R. Amin, J. Sander, J. De Coninck, A.P. Tomsia, Y.-M. Chiang, Impact of pore tortuosity on electrode kinetics in lithium battery electrodes: study in directionally freeze-cast $LiNi_{0.8}Co_{0.15}Al_{0.05}O_2$ (NCA), J. Electrochem. Soc. 165 (2018) A388–A395.

[21] P.A. Johns, M.R. Roberts, Y. Wakizaka, J.H. Sanders, J.R. Owen, How the

electrolyte limits fast discharge in nanostructured batteries and supercapacitors, Electrochem. Commun. 11 (2009) 2089–2092.
[22] T. Waldmann, B.-I. Hogg, M. Kasper, S. Grolleau, C.G. Couceiro, K. Trad, B.P. Matadi, M. Wohlfahrt-Mehrens, Interplay of operational parameters on lithium deposition in lithium-ion cells: systematic measurements with reconstructed 3-electrode pouch full cells, J. Electrochem. Soc. 163 (2016) A1232–A1238.
[23] C. Shen, D. Xiong, L.D. Ellis, K.L. Gering, L. Huang, J.R. Dahn, Using the charge-discharge cycling of positive electrode symmetric cells to find electrolyte/electrode combinations with minimum reactivity, J. Electrochem. Soc. 164 (2017) A3349–A3356.
[24] P. Ping, Q.S. Wang, J.H. Sun, X. Xia, J.R. Dahn, Studies of the effect of triphenyl phosphate on positive electrode symmetric Li-ion cells, J. Electrochem. Soc. 159 (2012) A1467–A1473.
[25] B.-S. Lee, Z. Wu, V. Petrova, X. Xing, H.-D. Lim, H. Liu, P. Liu, Analysis of rate-limiting factors in thick electrodes for electric vehicle applications, J. Electrochem. Soc. 165 (2018) A525–A533.
[26] J. Li, C. Daniel, S.J. An, D. Wood, Evaluation residual moisture in lithium-ion battery electrodes and its effect on electrode performance, MRS Adv. 1 (2016) 1029–1035.
[27] S.J. An, J. Li, C. Daniel, S. Kalnaus, D.L. Wood, Design and demonstration of three-electrode pouch cells for lithium-ion batteries, J. Electrochem. Soc. 164 (2017) A1755–A1764.
[28] S. Malifarge, B. Delobel, C. Delacourt, Determination of tortuosity using impedance spectra analysis of symmetric cell, J. Electrochem. Soc. 164 (2017) E3329–E3334.
[29] K. Xu, “Charge-transfer” process at graphite/electrolyte interface and the solvation sheath structure of Li + in nonaqueous electrolytes, J. Electrochem. Soc. 154 (2007) A162–A167.
[30] K.L. Browning, R.L. Sacci, G.M. Veith, Energetics of Na + transport through the electrode/cathode interface in single solvent electrolytes, J. Electrochem. Soc. 164 (2017) A580–A586.
[31] Y. Ishihara, K. Miyazaki, T. Fukutsuka, T. Abe, Kinetics of lithium-ion transfer at the Interface between $Li_4Ti_5O_{12}$ thin films and organic electrolytes, ECS Electrochem. Lett. 3 (2014) A83–A86.